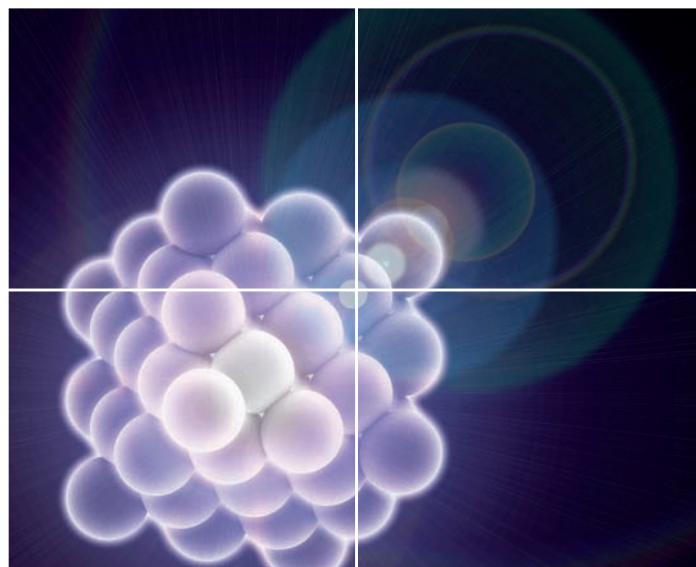


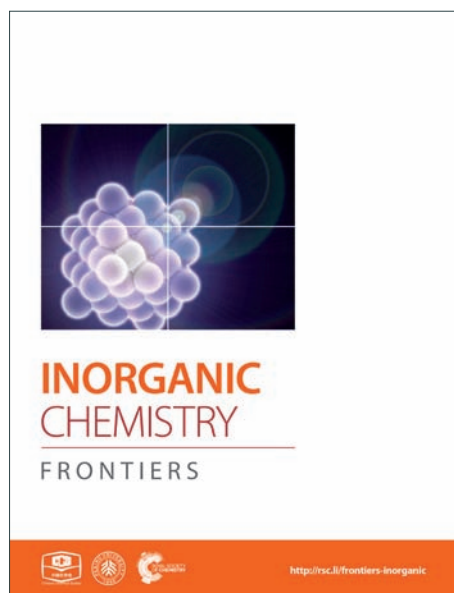
INORGANIC CHEMISTRY

FRONTIERS

Accepted Manuscript



This article can be cited before page numbers have been issued, to do this please use: A. Datta, K. Das, S. Nandi, S. mane, S. Mondal, C. Massera, C. Sinha, C. Hung, T. Askun, P. Celikboyun, Z. Canturk, E. Garribba and T. Akitsu, *Inorg. Chem. Front.*, 2015, DOI: 10.1039/C5QI00060B.



This is an *Accepted Manuscript*, which has been through the Royal Society of Chemistry peer review process and has been accepted for publication.

Accepted Manuscripts are published online shortly after acceptance, before technical editing, formatting and proof reading. Using this free service, authors can make their results available to the community, in citable form, before we publish the edited article. We will replace this *Accepted Manuscript* with the edited and formatted *Advance Article* as soon as it is available.

You can find more information about *Accepted Manuscripts* in the [Information for Authors](#).

Please note that technical editing may introduce minor changes to the text and/or graphics, which may alter content. The journal's standard [Terms & Conditions](#) and the [Ethical guidelines](#) still apply. In no event shall the Royal Society of Chemistry be held responsible for any errors or omissions in this *Accepted Manuscript* or any consequences arising from the use of any information it contains.

A Ni(II) Dinuclear Complex Bridged by End-on Azide-N and Phenolate-O**Atoms: Spectral Interpretation, Magnetism and Biological Study**

**Kuheli Das,^[a] Amitabha Datta,^[*,b] Soumendranath Nandi,^[a] Sandeep B. Mane,^[b]
Sudipa Mondal,^[a] Chiara Massera,^[c] Chittaranjan Sinha,^[*,a] Chen-Hsiung
Hung,^[*,b] Tulin Askun,^[d] Pinar Celikboyun,^[d] Zerrin Cantürk,^[e] Eugenio
Garribba,^[f] Takashiro Akitsu,^[g]**

^[a] Department of Chemistry, Jadavpur University, Kolkata – 700032, India

^[b] Institute of Chemistry, Academia Sinica, Taipei - 115, Taiwan

^[c] Dipartimento di Chimica, Università degli Studi di Parma, Viale delle Scienze,
17/A, 43124, Parma, Italy

^[d] Department of Biology, Faculty of Sciences and Arts, University of Balikesir,
Cagis Campus, 10145, Balikesir, Turkey

^[e] Department of Pharmaceutical Microbiology, Pharmacy Faculty, Anadolu
University, Yunusemre Campus, 26470, Eskisehir, Turkey

^[f] Dipartimento di Chimica e Farmacia, and Centro Interdisciplinare per lo Sviluppo
della Ricerca Biotecnologica e per lo Studio della Biodiversità della Sardegna,
Università di Sassari, Via Vienna 2, I-07100 Sassari, Italy

^[g] Department of Chemistry, Faculty of Science, Tokyo University of Science
1-3 Kagurazaka, Shinjuku-ku, Tokyo 162-8601, Japan

Corresponding authors. amitd_ju@yahoo.co.in (A. Datta), c_r_sinha@yahoo.com (C.
Sinha), chhung@gate.sinica.edu.tw (C.-H. Hung)

A potential tetradentate monoanionic N_2O_2 chelator, HL, derived from the condensation of *o*-vanillin and *N,N*-dimethylethylenediammine, has been reacted with nickel perchlorate and sodium azide, to yield the dinuclear Ni(II) complex $[Ni(L)(\mu_{1,1}-N_3)Ni(L)(OH_2)_2].ClO_4$ (**1**), where $L = Me_2N(CH_2)_2N=CH-C_6H_3(O^-)(OCH_3)$. The complex has been characterized by X-ray diffraction analysis and different spectroscopic techniques. The coordination geometry around the Ni(II) centres is a distorted octahedron, with the azide ligand and the phenolato oxygen atom bridging in a $\mu_{1,1}$ and μ_2 mode, respectively. The EPR spectra, recorded at liquid nitrogen (77 K) and room temperature (298 K), show *g* factors at 2.080 and 2.085, in agreement with the structure determined by X-ray diffraction analysis. The VTM study confirms that there is a ferromagnetic interactions between the bridging binuclear Ni(II) ions ($S=1$). The evaluation of cytotoxic effects on different human cancer cell lines (A-549, MCF-7 and CaCo-2) suggests that both the ligand and complex **1** have potential anticancer properties. Furthermore, they also exhibit anti-mycobacterial activity against *M. tuberculosis* H37Rv (ATCC 27294) and *M. tuberculosis* H37Ra (ATCC 25177) strains. Molecular docking of HL with the enoyl acyl carrier protein reductase of *M. tuberculosis* H37R_v (PDB ID: 4U0K) has been examined, showing that HL forms two hydrogen bonds with Lys165 (1.94 and 2.53 Å) in its best docked pose.

Introduction

Metal complexes containing Schiff-base ligands derived from aromatic carbonyl compounds have been widely studied in connection with metallo-protein models because of the versatility of their steric and electronic properties, which can be fine-tuned by choosing the appropriate amine precursors and ring substituents.¹ It has been recognized that the metal centres and the binding Schiff base ligands (as anions or capping molecules) may play important roles in the formation of desirable compounds, due to their different molecular shape, charge and size.² Besides, also coligands can be used to adjust the properties of the resulting compounds. Several pseudohalide-bridged metal complexes with various Schiff bases continue to be the subject of much interest, and intensive investigations have taken place to shed light on their diverse structures and potential applications as magnetic materials.³ Among the pseudohalides, the azido group has received much attention due to its versatility as a bridging ligand and to the wide variety of magnetic properties shown by its compounds. The versatile azide ion, which can indeed form dimers, clusters, and polymers exhibiting significant magnetic properties such as ferro- and antiferromagnetic interactions, has been extensively used because it may induce interesting magnetic couplings by two different bonding modes, *i.e.* end-on ($\mu_{1,1}$ ferromagnetic) and end-to-end ($\mu_{1,3}$ antiferromagnetic).⁴ It is worth reporting that the ferromagnetic ordering between the metal centres induced by the end-on or 1,1-coordination mode is reduced if the bridging bite angle exceeds 108° .⁵ The chemistry of nickel complexes with multidentate Schiff base ligands has also attracted huge attention; indeed, magnetic exchange interactions between metal centres in binuclear nickel salts continue to be a subject of wide interest, with particular emphasis on

determining magnetic structural correlations.⁶ Many structural parameters affect the superexchange mechanism in these sorts of dimers.⁷ Kahn⁸ has suggested that the exchange integral is the sum of two antagonistic interactions favoring the antiferromagnetic and ferromagnetic interactions.

Nickel complexes play an important role in bioinorganic chemistry and may provide the basis of models for active sites of biological systems or act as catalysts.⁹ Tuberculosis, an infectious and chronically bacterial disease, caused primarily by the bacillus *Mycobacterium tuberculosis* and rarely by *M. bovis* and *M. africanum*, effects lung (pulmonary TB) and even can spread to the other organs (extra pulmonary TB).¹⁰ Million children has died per year from this disease.¹¹ Mycobacteria resist (multidrug resistant or MDR-TB) to many of chemicals, disinfectants, antibiotics and chemotherapeutical agents.¹² Synthetic chemistry research is now directed to explore the synergistic relations between natural products and synthetic drugs for better treatment. Cytotoxicity assays are widely used in bio-inorganic chemistry to screen for cytotoxicity in compound libraries. Assessing cell membrane integrity is one of the most common ways to measure cell viability and cytotoxic effects. The control of tumor cell proliferation by inhibition of the cell cycle and induction of apoptosis could provide a therapeutic strategy for the treatment of cancer.¹³ Programmed cell death plays an important role in the regulation of cellular homeostasis.¹⁴ Marin-Hernandez et al.¹⁵ indicated that some mixed chelate transition metal-based drugs have more potent antitumor activity than cisplatin in in vivo and in vitro studies of a variety of tumor cells. However, human cancer cell lines are a useful model to study cell growth inhibition of tumor cells by natural compounds or newly synthesized compounds.

Recently, a unique example of bridge distance dependency of the exchange interaction has emerged from the magnetic properties of a μ -phenoxo- $\mu_{1,1}$ -N₃ dinickel(II) compound.¹⁶ In our present contribution, we report the structural description and DFT computation analysis of the Ni(II) derivative [Ni(L)($\mu_{1,1}$ -N₃)Ni(L)(OH₂)₂].ClO₄ (**1**), where L = Me₂N(CH₂)₂N=CH-C₆H₃(O⁻)(OCH₃)¹⁷; additionally the spectral properties and temperature-dependent magnetic behaviour of the complex are elucidated. Both the ligand HL and complex **1** exhibit anti-mycobacterial activity on *M. tuberculosis* H37Rv (ATCC 27294) and *M. tuberculosis* H37Ra (ATCC 25177) strains. The anti-micobacterial efficiency of HL has been examined by molecular docking with the enoyl acyl carrier protein reductase of *M. tuberculosis* H37Rv (PDB ID: 4U0K) and has been compared with the first line drug isoniazide.

Experimental

Materials

o-Vanillin and 2-dimethylaminoethylamine (Merck), and sodium azide (Sigma-Aldrich) were purchased and used as received without further purification. Hydrated nickel(II) perchlorate was prepared by the treatment of nickel(II) carbonate basic hydrate, NiCO₃·2Ni(OH)₂ (AR grade, E. Merck), with perchloric acid (AR grade, E. Merck), followed by slow evaporation on a steam bath. It was then filtered through a fine glass frit and stored in CaCl₂ desiccators. All solvents used were of reagent grade. The ligand (HL) synthesis was carried out following the published procedure.¹⁷

Physical measurements

Microanalytical data (C, H, and N) were collected on a Perkin–Elmer 2400 CHNS/O elemental analyzer. FTIR spectra were recorded on a Perkin-Elmer RX-1 spectrophotometer in the range 4000–400 cm^{-1} as KBr pellets. Electronic spectra were measured on a Lambda 25 (U.V.–Vis.–N.I.R.) spectrophotometer in methanol. Emission spectra were examined with a LS 55 Perkin–Elmer spectrofluorometer at room temperature (298 K) in different solutions under degassed conditions. The fluorescence quantum yield of the complexes was determined using carbazole as a reference with known Φ_R of 0.42 in benzene.¹⁸ The complex and the reference dye were excited at same wavelength, maintaining nearly equal absorbance (~ 0.1), and the emission spectra were recorded. The area of the emission spectrum was integrated using the software available in the instrument and the quantum yield was calculated according to the following equation:

$$\frac{\phi_s}{\phi_R} = \left[\frac{A_s}{A_R} \right] \times \left[\frac{(Abs)_R}{(Abs)_S} \right] \times \left[\frac{\eta_S^2}{\eta_R^2} \right]$$

Here, Φ_S and Φ_R are the fluorescence quantum yield of the sample and reference, respectively. A_S and A_R are the area under the fluorescence spectra of the sample and the reference, respectively, $(Abs)_S$ and $(Abs)_R$ are the respective optical densities of the sample and the reference solution at the wavelength of excitation, and η_S and η_R are the values of refractive index for the respective solvent used for the sample and reference. EPR spectra were recorded from 0 to 10000 Gauss in the temperature range 77–298 K with an X-band (9.4 GHz) Bruker EMX spectrometer equipped with an HP 53150A microwave frequency counter. Magnetic properties were investigated with a Quantum Design MPMS-XL superconducting quantum interference device magnetometer (SQUID) at an applied field 10000 Oe in a

temperature range 5-300 K. Diamagnetic correction was carried out by using Pascal constants.

Synthesis of the ligand, HL

The ligand, HL, 2-[[2-(dimethylamino)ethyl]imino]methyl]-6-methoxyphenol was prepared¹⁷ by condensation of *o*-vanillin (0.152 g, 1.0 mmol) with 2-dimethylaminoethylamine (0.109 ml, 1 mmol) in methanol (15 mL). After 2 h reflux, the pale yellow methanolic solution was cooled down to room temperature. The solvent was removed under reduced pressure, and the Schiff-base ligand was obtained as a light-yellow liquid that was used without further purification. ¹H NMR (TMS, CDCl₃) δ: 12.80 (1H, s, H-1), 9.90 (1H, s, H-6,6'), 6.46-6.86 (3H, d & t, Ar-H), 3.86 (3H, s, H-6), 3.45 (2H, t, J = 4.5 Hz, H-7), 3.72 (2H, t, J = 3.4 Hz, H-8), 2.29 (6H, s, H-9) ppm (see ESI, **Figure S1**).

Synthesis of the complex (1)

Upon addition of HL (1 mmol) in methanol (20 mL) to Ni(ClO₄)₂·6H₂O (0.36 g, 1 mmol) in the same solvent the mixture was stirred for half an hour and then a solution of NaN₃ (0.03 g, 0.5 mmol) in the minimum volume of water was added, and the reaction mixture was kept undisturbed and allowed to evaporate slowly. After ten days, dark brown, rectangular-shaped single crystals of **1** were obtained. The crystals were filtered off, washed with water and dried in air. Yield: 71%. Anal. Calc. for C₂₄H₄₂Ni₂N₇O₁₂Cl: C, 37.23; H, 5.47; N, 12.67. Found: C, 37.73; H, 5.09; N, 12.83%.

X-ray crystallography

The crystal structure of complex **1** was determined by X-ray diffraction methods. Crystal data and experimental details for data collection and structure refinement are reported in **Table 1**. Intensity data and cell parameters were recorded at 293(2) K on a Bruker Breeze (MoK α radiation = 0.71069 Å) equipped with a CCD area detector and a graphite monochromator. No significant crystal decay was observed. The raw frame data were processed using SAINT and SADABS to yield the reflection data file.²⁰ The structure was solved by Direct Methods using the SIR97 program²¹ and refined on F_o^2 by full-matrix least-squares procedures, using the SHELXL-97 program²² in the WinGX suite v.1.80.05.²³ All non-hydrogen atoms were refined with anisotropic atomic displacements with the exception of the oxygen atoms of the perchlorate ion and the oxygen atoms of the lattice water molecules. The hydrogen atoms were included in the refinement at idealized geometry (C-H 0.95 Å) and refined “riding” on the corresponding parent atoms. The weighting scheme used in the last cycle of refinement was $w = 1/[\sigma^2 F_o^2 + (1016)^2]$, where $P = (F_o^2 + 2F_c^2)/3$. Crystallographic data (excluding structure factors) for the structure reported have been deposited with the Cambridge Crystallographic Data Centre as supplementary publication no. CCDC-894363 and can be obtained free of charge on application to the CCDC, 12 Union Road, Cambridge, CB2 IEZ, UK (fax: +44-1223-336-033; e-mail deposit@ccdc.cam.ac.uk or <http://www.ccdc.cam.ac.uk>).

Table 1. Crystallographic data of complex 1.

Empirical formula	C ₂₄ H ₄₂ ClN ₇ O ₁₂ Ni ₂
Formula weight	773.52
Temperature	293(2)
Wavelength (Å)	0.71069
Crystal system	Monoclinic
Space group	<i>P</i> 21
<i>a</i> , Å	11.748(2)
<i>b</i> , Å	11.093(1)
<i>c</i> , Å	13.278(2)
β , deg	100.963(2)
Volume, Å ³	1698.8(4)
<i>Z</i>	2
D _{calc} (mg m ⁻³)	1.512
μ (Mo K α) (mm ⁻¹)	1.254
F(000)	808
θ range for data collection	1.56–28.34
Reflections collected / unique	24015 / 8462 [<i>R</i> (<i>int</i>) = 0.0416]
Observed reflections [<i>F</i> _o > 4 σ (<i>F</i> _o)]	5861
Data / restraints / parameters	8462 / 4 / 390
Goodness-of-fit on <i>F</i> ^{2a}	0.991
Final <i>R</i> indices [<i>F</i> _o > 4 σ (<i>F</i> _o)] ^b	<i>R</i> 1 = 0.0543, <i>wR</i> 2 = 0.1408
<i>R</i> indices (all data)	<i>R</i> 1 = 0.0882, <i>wR</i> 2 = 0.1641
Largest diff. Peak and hole, e.Å ⁻³	0.687 and -0.663

^aGoodness-of-fit $S = [\sum w(F_o^2 - F_c^2)^2 / (n-p)]^{1/2}$, where *n* is the number of reflections and *p* the number of parameters. ^b $R_1 = \sum \|F_o - F_c\| / \sum F_o$, $wR_2 = [\sum w(F_o^2 - F_c^2)^2 / \sum w(F_o^2)]^{1/2}$.

Theoretical calculations

Full geometry optimization of **1** and **2** were carried out using density functional theory (DFT) at the B3LYP level.²⁴ All calculations were performed using the Gaussian 03 program package²⁵ with the aid of the Gauss View visualization program.²⁶ For C, H, N, O, and Cl the 6-31G(d) basis set were assigned, while for Cu and Ni the LanL2DZ basis set with effective core potential were employed.²⁷ The vibrational frequency calculations were performed to ensure that the optimized geometries represent the local minima and there are only positive Eigen values. Vertical electronic excitations based on B3LYP optimized geometries were computed using the time-dependent density functional theory (TD-DFT) formalism²⁸⁻³⁰ in acetonitrile using conductor-like polarizable continuum model (CPCM).³¹ Gauss Sum was used to calculate the fractional contributions of various groups to each molecular orbital.³²

Anti-mycobacterial activity

Microorganisms. In the antimycobacterial assay, *M. tuberculosis* H₃₇Rv (ATCC 27294), *M. tuberculosis* H₃₇Ra (ATCC 25177) strains and two clinical strains (strain-1 and strain-2) obtained from the hospital were used.

Medium. In the assays, Mycobacteria Growth Indicator Tubes (MGIT) and their supplements, BBL MGIT OADC enrichment and BBL MGIT PANTA were purchased from BD. The MGIT Mycobacteria Growth Indicator Tube contains 4 mL of modified Middlebrook 7H9 Broth base.

Inoculum preparation. For the cultivation of mycobacteria, the MGIT (Mycobacteria Growth Indicator Tube), a fluorescent compound is embedded in silicone on the bottom, then 4 mL of modified Middle brook 7H9 Broth base are added to the mixture. After that 0.5 mL of OADC enrichment, (an oleic acid, albumin, dextrose and catalase) and PANTA antibiotic mixture to prevent the proliferation of any non-mycobacteria (0.1 mL) are added to this medium. Tubes are incubated at 37 °C. For positive control, MGIT tubes are prepared by inoculating bacteria and tube reading starts on the second day of incubation using a Micro MGIT fluorescence reader which has a long wave UV light.³³ To prepare the inoculum the positive tubes (day 1 or day 2 positive) are used directly as inoculums. The positive tubes between day 3 and day 5 are diluted to 1:4 ratio by sterile saline. Inoculums, prepared from a Day 1 to Day 5 MGIT 7 mL positive tube, range between 0.8×10^5 and 3.2×10^5 CFU/mL. Each assay is performed according to the MGIT manual fluorometric susceptibility test procedure recommended by the manufacturer.^{33,34}

Antimycobacterial susceptibility assay. The activity of the ligand, HL and complex **1** against *M. tuberculosis* strains was tested using the Microplate Presto Blue Assay (MPBA) with the method described by Collins & Franzblau³⁵ and modified by Jimenez-Arellanes et al.³⁶ 100 µl of compound was transferred in the first column; then 100 µl of 7H9 broth was transferred from column 1 to column 10. Column 11 and 12 were negative and positive control respectively. 100 µl of compound were transferred from column 1 to column 2. Then it was mixed by pipettes three times; the procedure was repeated to provide serial 1:2 dilutions. 100 µl of excess medium was discarded from the wells in column 10. Final test concentration ranges were 512-1 µg/ml in the mixture. Microplates were inoculated with the bacterial suspension (20

μL per well) except for the negative control and incubated at 37 °C for 6 days. Presto blue (15 μL , Life Technologies) was then added to the bacterial growth control wells (without compound) and the microplates were incubated at 37 °C for an additional 24 h. If the dye turned from blue to pink/red (indicating positive bacterial growth); the Presto blue solution was added to the other wells to determine the MIC values. All tests were performed in triplicate. The minimal inhibitory concentration (MIC) was defined as the lowest concentration of sample that prevents a colour change to pink/red. To determine the minimal bactericidal concentration (MBC) values, MIC concentrations-wells and higher concentrations wells were used. Each well transferred into fresh 7H9 broth (185 μL) and added a mycobacterial suspension (15 μL). Plates were incubated at 37 °C for 6 days. The MBC corresponded to the minimum compound concentration which does not cause a colour change in the cultures when re-incubated in fresh medium.³⁷ Streptomycin (STR), ethambutol (EMB), Rifampicin (RFP) and isoniazid (INH) were used as standard drugs.

Cytotoxicity study

Cell culture. A-549 (non-small cell lung cancer), MCF-7 (breast cancer), Caco-2 (colon cancer cell line) and healthy cell lines, CRL-2522 (human normal fibroblast); were used in the study, provided by ATCC cell bank. The cells were grown in RPMI 1640 medium supplemented with 2 mM L-glutamine and 10% fetal bovine serum, 1% penicillin-streptomycin at a temperature of 37 °C in a humidified incubator with a 5% CO₂ atmosphere.

Cell viability test by MTT assay. MTT [3-(4,5-dimethylthiazol-2-yl)-2,5-diphenyl tetrazolium bromide] assay was performed to determine the effect of the ligand, HL

and complex **1**; the following concentrations, (500, 250, 125, 62.5, 31.25, 15.625, 7.8125, 3.9, 1.95, 0.97 $\mu\text{g/ml}$) were seeded on 5×10^3 cells which were cultivated in each well of the plate with 96 wells. After 24 hours of incubation, 0.1 ml MTT working solution (0.5 mg/mL) was added to each well and they were let to incubation at 37 °C in a 5% CO₂ incubator for 3-4 hours. After that, the unreacted dye was removed and the insoluble formazan crystals were dissolved in DMSO. The absorbance intensity of the living cell on the plate was measured in ELISA device (Cytation3, Biotek, USA) in 540 nm (1). Acquired absorbance values corresponded to metabolic activities in the cells in culture media. Because this value was correlated to the number of living cells, the results were expressed in liveliness percent and calculated using the formula below;

$$\text{Liveliness percent} = \frac{100}{\frac{\text{Absorbance of the control}}{\text{Absorbance of the sample}}}$$

Docking studies

Molecular docking is used to predict how a protein interacts with small molecules. The crystal structure of the enoyl acyl carrier protein reductase of *M. tuberculosis* H37R_v was downloaded from the RCSB protein data bank (<http://www.pdb.org>) and used for docking. The protein (PDB id : 4U0K) was co-crystallized with (3S)-N-(5-chloro-2-methylphenyl)-1-cyclohexyl-5-oxopyrrolidine-3-carboxamide and nicotinamide-adenine-dinucleotide. *In silico* docking studies were performed using the CDOCKER module of the Receptor-Ligand interactions protocol section of Discovery Studio client 3.5.³⁹ Initially there was a pre-treatment process for the protein and the ligand. The structure of the ligand was drawn in Chemdraw 5.0, saved in .mol file and finally the .mol file was imported to the Discovery studio 4.0

platform. The ligand preparation was done using the Prepare Ligand module in the Receptor-Ligand interactions tool of Discovery studio 4.0 and the prepared ligand was hence used for docking. The protein preparation was done under the Prepare Protein module of the Receptor-Ligand interactions tool of Discovery Studio 4.0 and that was used for docking. We subsequently defined the protein as total receptor and the active site was selected based on the ligand binding domain of (3S)-N-(5-chloro-2-methylphenyl)-1-cyclohexyl-5-oxopyrrolidine-3-carboxamide and nicotinamide-adenine-dinucleotide. Then the pre-existing ligand was removed and the prepared ligand was placed instead. The most favourable docked pose was selected according to the minimum free energy of the protein-ligand complex and analysed to investigate the interaction.

ADMET prediction

Absorption, distribution, metabolism, excretion and toxicity (ADMET) predictions were done in the ADMET descriptor module of the Small molecules protocol of Discovery studio client 4.0. Also the druglikeness of the compounds were checked following Lipinski's rule of five.^{40,41}

Results and discussion

Synthesis and formulation

The monoanionic Schiff base precursor [(2-[(2-(dimethylamino)ethyl]imino)methyl]-6-methoxyphenol] (HL), was prepared by the condensation of *o*-vanillin and *N,N*-dimethylethylenediamine (1:1 mole proportion) in methanol. HL was then reacted with Ni(ClO₄)₂·6H₂O and NaN₃ in a methanol/water

mixture to yield $[\text{Ni}(\text{L})(\mu_{1,1}\text{-N}_3)\text{Ni}(\text{L})(\text{OH}_2)_2]\cdot\text{ClO}_4$ (**1**), where $\text{L} = \text{Me}_2\text{N}(\text{CH}_2)_2\text{N}=\text{CH}-\text{C}_6\text{H}_3(\text{O}^-)(\text{OCH}_3)$, by slow evaporation of the solvent. The ^1H NMR spectrum of HL shows singlet signals at δ 12.80 and 9.90 ppm for -OH and -CH=N protons, respectively. Furthermore, the singlet signals at δ 3.86 ppm and 2.29 ppm refer to $-\text{OCH}_3$ and $-\text{N}(\text{CH}_3)_2$ protons. In addition, two triplet signals at δ 3.45 and 3.07 ppm are assigned to 7-H and 8-H protons with J value 4.5 and 3.4 Hz respectively. The corresponding aromatic protons appear as doublet and triplet in the region 6.46-6.86 ppm. The FTIR spectrum of the free ligand shows bands at 3436 cm^{-1} and 1660 cm^{-1} which are due to the stretching frequencies of $\nu(\text{O-H})$ and $\nu(\text{C=N})$ respectively. The two $\nu(\text{C-O})$ bands for C-OH and C-OMe are perceived at 1260 and 1086 cm^{-1} respectively.⁴² In complex, a distinct band appears at 1634 cm^{-1} corresponding to the azomethine (C=N) functional group.⁴³ The lowering of the stretching frequency from 1660 to 1634 cm^{-1} indicates the coordination to the metal center. The $\nu(\text{C-O})$ band is shifted to 1217 cm^{-1} on complexation. Furthermore, the complex shows one sharp band at 2072 cm^{-1} , which indicates the presence of N_3 as bridging ligand. Bands in agreement with the non-coordinated perchlorate anion could also be observed at 1110 cm^{-1} alongwith a weak shoulder at 629 cm^{-1} . The $\nu_{(\text{M-N})}$ and $\nu_{(\text{M-O})}$ stretching frequencies are observed at 462 , 339 and 278 cm^{-1} .

Crystal structure

The molecular structure of the dinuclear nickel compound $[\text{Ni}(\text{L})(\mu_{1,1}\text{-N}_3)\text{Ni}(\text{L})(\text{OH}_2)_2]\text{ClO}_4\cdot 2\text{H}_2\text{O}$ (**1**) is shown in **Figure 1** (for the ortep view with complete labeling scheme see ESI, Figure S2). Relevant bond lengths and angles are given in **Table 2**. The cationic complex comprises two nickel(II) ions, two mono

deprotonated [(2-[2-(dimethylamino)ethyl]imino)methyl]-6-methoxyphenol] ligands (tagged with labels A and B) roughly perpendicular one to the other, a bridging azide anion and two water molecules.

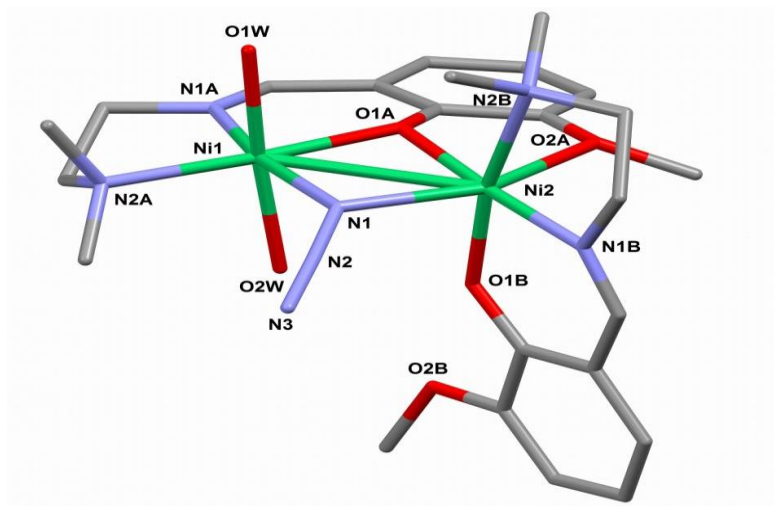


Figure 1. Molecular structure of the cationic complex **1** with partial labeling scheme. The perchlorate anion and the lattice water molecules have been omitted for clarity. The two ligands are tagged with labels A and B.

The dimer is assembled *via* the μ_2 -nitrogen atom N1 of the azide anion and the μ_2 -oxygen atom O1A of ligand A. Each metal center is in an octahedral NiN_3O_3 environment (more distorted for Ni2) but provided by a different set of ligands. Indeed, in the case of Ni1, only the Schiff base A is involved in the coordination; the equatorial plane is occupied by the imino and amino nitrogen atoms N1A and N2A, by the bridging nitrogen atom N1 of the azide anion and by the bridging phenolato oxygen O1A. The coordination is completed by two water oxygen atoms in apical position. Ni2, which, on the contrary, does not coordinate any water molecule, is chelated by both ligand A and B. In particular, considering the plane passing through

ligand A as the equatorial plane, the metal center is surrounded by the bridging atoms O1A and N1, by the methoxy oxygen atom O2A and by the imino nitrogen atom N1B. In this case the apical positions are this time occupied by the amino nitrogen N2B and by the phenolate oxygen O1B. The potentially coordinating oxygen O2B remains dangling without taking part in any interaction.

Table 2. Selected bond lengths [Å] and angles [°] for complex 1.

Ni1-O1A	1.997(4)	Ni2-O1B	2.005(3)	N2A-Ni1-O1A	173.29(9)
Ni1-N1A	2.020(8)	Ni2-N1B	1.999(6)	N1A-Ni1-N1	167.37(9)
Ni1-N2A	2.129(7)	Ni2-N2B	2.156(4)	O1W-Ni1-O2W	173.89(9)
Ni1-N1	2.117(5)	Ni2-N1	2.145(5)	N2B-Ni2-O1B	170.42(9)
Ni1-O1W	2.116(4)	Ni2-O1A	2.000(5)	O2A-Ni2-N1	153.10(9)
Ni1-O2W	2.119(4)	Ni2-O2A	2.275(5)	N1B-Ni2-O1A	174.80(9)
Ni1-Ni2	3.168(2)	Ni1-N1-Ni2	96.04(9)	Ni1-O1A-Ni2	104.87(9)

The crystal structure is stabilized by a network of hydrogen bonds (relevant geometrical parameters are reported in **Table 3**) comprising the perchlorate anion, the coordinated and lattice water molecules, and the azide ligand. In particular, the complexes form a 1D supramolecular chain along the *b* direction of the unit cell through the O2W...N3 H-bond, involving one of the water molecules coordinated to Ni1 and the terminal nitrogen atom of the azide ligand bridging the two nickel centers (see **Figure 2**). These chains are in turn connected by means of the hydrogen bonds involving the coordinated water molecule O1W, the lattice water molecules O3W and O4W, and the perchlorate anion (**Figure 3**).

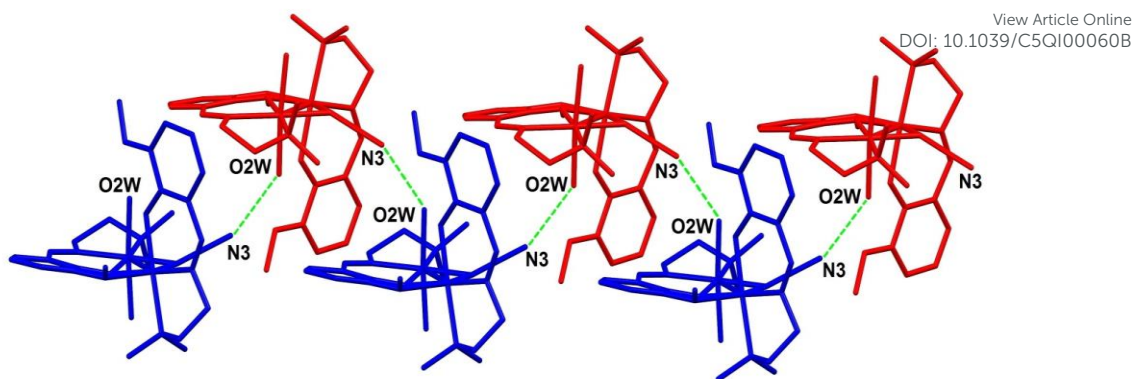


Figure 2. Representation of the 1D supramolecular chain formed through H-bond interactions (green dotted lines) between the water oxygen O2W and the azide nitrogen N3.

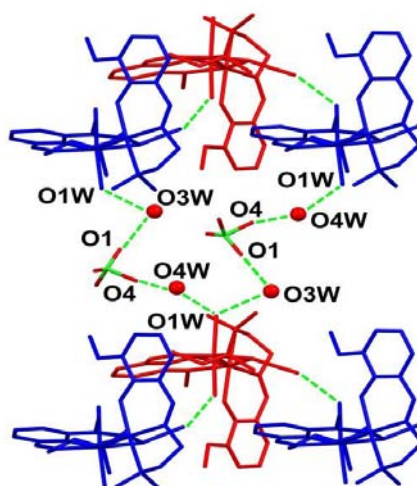


Figure 3. The network of hydrogen bonds connecting adjacent chains in the lattice.

Table 3. Relevant geometrical parameters for the hydrogen bonds in complex 1.

O2W⋯N3	2.99(1)	O1⋯O3W	2.78(2)
O1W⋯O3W	2.86(1)	O4⋯O4W	2.35(2)
O1W⋯O4W	2.75(1)		

Electronic spectra

The peaks in the electronic spectrum of complex **1** in methanol, are similar, exhibiting d-d maxima typical of octahedral Ni^{II}.⁴⁴ In the ligand, the maximum absorption bands are ascertained at 232 and 315 nm which may arise due to $\pi \rightarrow \pi^*$ and $n \rightarrow \pi^*$ transitions. On complexation, the corresponding $\pi \rightarrow \pi^*$ and $n \rightarrow \pi^*$ bands are shifted from 235 to 282 nm and 315 to 382 nm, respectively (see ESI, **Figure S3**). The characteristic d-d band for a Ni(II) complex is recognised at 410 and 635 nm.

The spectral properties are explained by the DFT computation of the optimized structure of complex **1**. The orbital energies along with the contributions from the ligands and the metal for selected MOs are given in **Figure 4** (see details in ESI, **Table S1**). Although the orbital contribution of the ligands (L and H₂O) predominates in most cases in both filled and vacant MOs LUMO+1, LUMO+8 and HOMO-10 show a higher metal contribution. In the complex, it is observed that the occupied MOs HOMO, HOMO-3 and HOMO-6 and the unoccupied MOs from LUMO+3 to LUMO+7 have all more than 60% ligand contribution. Similarly, also the water contribution is significant in complex **1**, being ~60% for the MOs HOMO-1, HOMO-2, HOMO-4, HOMO-5 and LUMO. The contribution of the bridging ligand azide is almost insignificant in both occupied and unoccupied MOs with the exception of LUMO+9 which contains a 60% azide function. In the complex Ni contributes in an irregular fashion: 7% to HOMO, 15% to HOMO-1, 16% to HOMO-3, 8% to HOMO-7, 44% HOMO-11 and 8% to LUMO, 42% to LUMO+1, 38% to LUMO+2, 38% to LUMO+3, 60% to LUMO+8 etc. Thus it is the ligands L and H₂O that mainly control the molecular orbitals and hence the spectral properties of the complex. Therefore HOMO \rightarrow LUMO is considered as L(π) \rightarrow H₂O(π^*); HOMO-3 \rightarrow LUMO+3 is LLCT involving L function (L(π) \rightarrow L(π^*)) whereas HOMO-1 \rightarrow

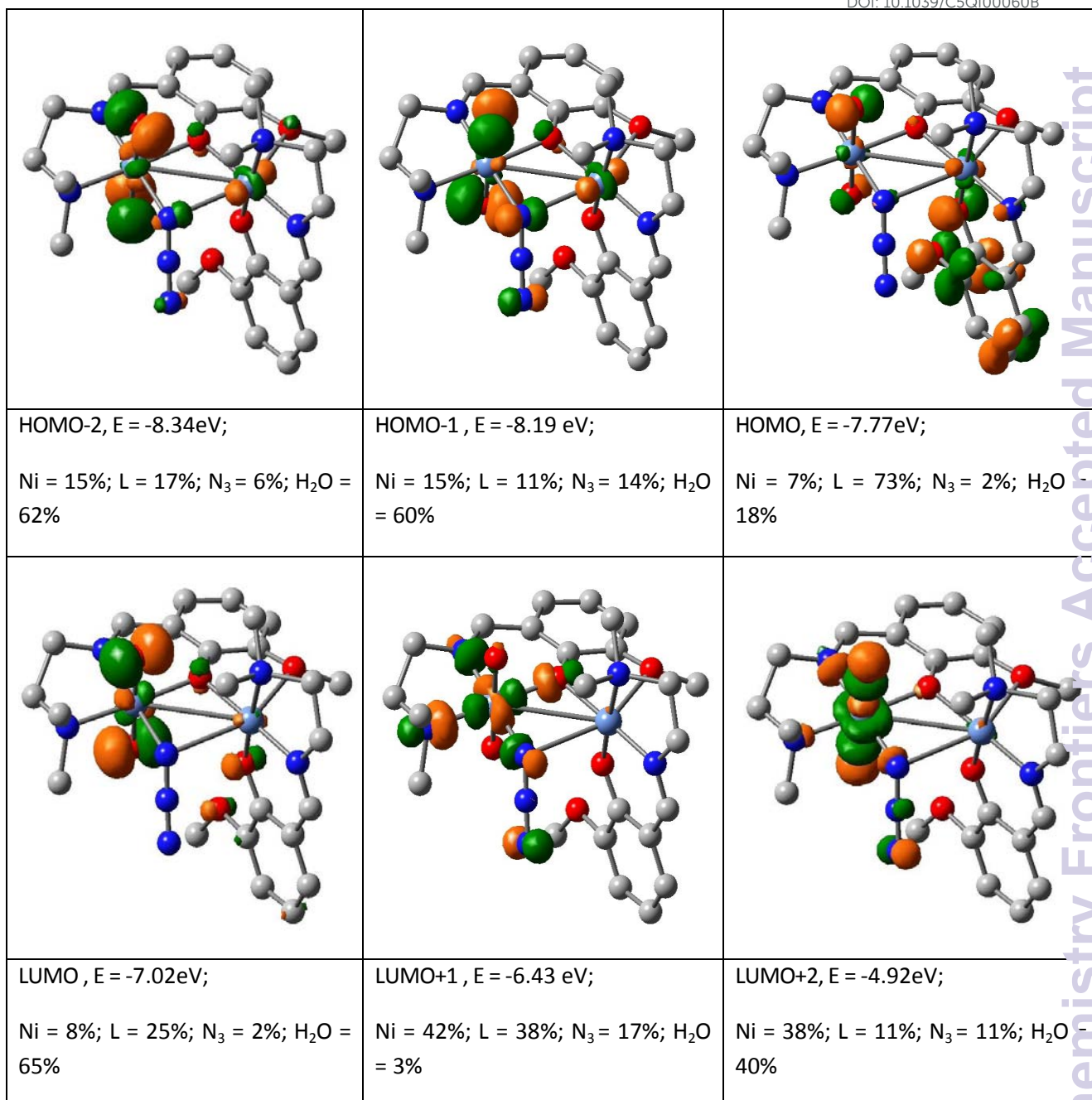


Figure 4. Contour plots of some selected MOs of $[\text{Ni}(\text{L})(\mu_{1,1}\text{N}_3)\text{Ni}(\text{L})(\text{OH}_2)_2]\cdot\text{ClO}_4$.

LUMO+8 is designated as LMCT transition ($\text{H}_2\text{O}(\pi) \rightarrow \text{Ni}(\text{d}\pi)$) and HOMO-11 \rightarrow LUMO is depicted as MLCT ($\text{Ni}(\text{d}\pi) \rightarrow \text{H}_2\text{O}(\pi^*)$). The calculated transitions are grouped in **Table 4**. The intensity of these transitions has been assessed from the oscillator strength (f). In methanol, the longest wavelength band calculated at >650 nm (f , 0.0100) for **1** is assigned to the $\text{Ni}(\text{d}\pi) \rightarrow \text{H}_2\text{O}(\pi^*)$ transition followed by a high intense transition at 411 nm (f , 0.0102) which is LLCT ($\text{L}(\pi) \rightarrow \text{L}(\pi^*)$) in nature. The other bands at 385 and 283 nm are LLCT in character whereas the high intensity band at 234 nm (f , 0.1510) is referred to the $\text{H}_2\text{O}(\pi) \rightarrow \text{Ni}(\text{d}\pi)$ transition.

Table 4. TD-DFT data of $[\text{Ni}(\text{L})(\mu_{1,1}\text{-N}_3)\text{Ni}(\text{L})(\text{OH}_2)_2]\cdot\text{ClO}_4$.

Excitation energy(ev)	Wavelength (nm)	f	Key Transitions	Character	Assignment
1.9019	651.90	0.0100	(32%) HOMO-11 \rightarrow LUMO	$\text{Ni}(\text{d}\pi) \rightarrow \text{H}_2\text{O}(\pi^*)$	MLCT
3.0144	411.31	0.0102	(62%) HOMO \rightarrow LUMO+5	$\text{L}(\pi) \rightarrow \text{L}(\pi^*)$	LLCT
3.2141	385.75	0.0134	(30%) HOMO-3 \rightarrow LUMO+3	$\text{L}(\pi) \rightarrow \text{L}(\pi^*)$	LLCT
3.8999	317.92	0.0690	(18%) HOMO-7 \rightarrow LUMO+3	$\text{H}_2\text{O}(\pi) \rightarrow \text{L}(\pi^*)$	LLCT
4.3694	283.76	0.0152	(68%)HOMO-13 \rightarrow LUMO+2	$\text{L}(\pi) \rightarrow \text{H}_2\text{O}(\pi^*)$	LLCT
5.2873	234.49	0.1510	(9%) HOMO-1 \rightarrow LUMO+8	$\text{H}_2\text{O}(\pi) \rightarrow \text{Ni}(\text{d}\pi)$	LMCT

LLCT ($\text{L}(\pi) \rightarrow \text{L}(\pi^*)$); MLCT (metal to ligand charge transfer: LLCT (ligand to Ligand charge transfer); LMCT (ligand to metal charge transfer)

Emission spectra

Fluorescence studies of the ligand HL and of complex **1** were carried out in methanol and the corresponding diagram is depicted in **Figure 5**. The emission bands of HL are observed at 364 and 423-445 nm exciting the $\pi \rightarrow \pi^*$ band while the maximum emission is found at 423 nm upon excitation at 315 nm. Complex **1** exhibits very low fluorescence efficiency when it is excited at the $\pi \rightarrow \pi^*$ transition and the maximum intensity is originated at 419 nm on $\lambda_{\text{exc}} = 281$ nm. No emission bands are detected at higher wavelength (>400nm). The fluorescence quantum yield of the ligand and complex was determined using carbazole as reference with known quantum yield value in benzene ($\Phi_{\text{R}} = 0.42$). The fluorescence quantum yield of the complex corresponds to a $\pi \rightarrow \pi^*$ transition band at 281 nm which is lower (0.005) than that of the ligand (0.022). This indicates the presence of energy transfer between the metal ion and the fluorophore ligand which coincides with a strong quenching of fluorescence.⁴⁵

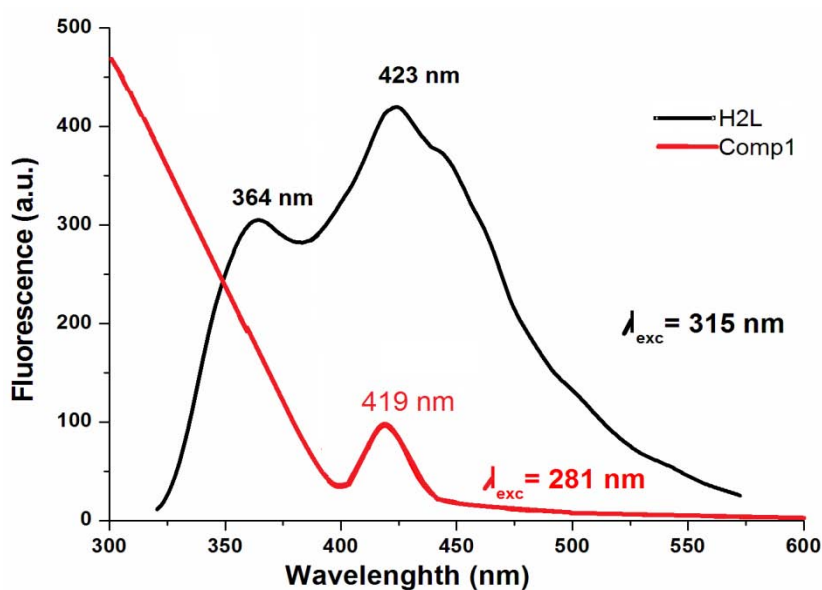


Figure 5. Emission spectra of HL (black curve, in DMF) and of the Ni(II) complex (**1**) (red curve, in MeOH).

EPR spectra

EPR spectra of the polycrystalline complex **1** were recorded at liquid nitrogen (77 K) and room temperature (298 K). The spectra are shown in **Figure 6**. Ni(II) has a d^8 configuration and its EPR spectra can be interpreted using a $S = 1$ spin Hamiltonian. Even if it does not possess a Kramer doublet as the lowest state in a magnetic field, usually spectra can be recorded for octahedral complexes.⁴⁶ The spectra reported in the traces a and b of **Figure 6** can be interpreted with nearly isotropic g tensor with g factor at 2.158 and 2.085 (298 K, trace a) and at 2.182 and 2.080 (77 K, trace b), in agreement with the structure determined by X-ray diffraction analysis.

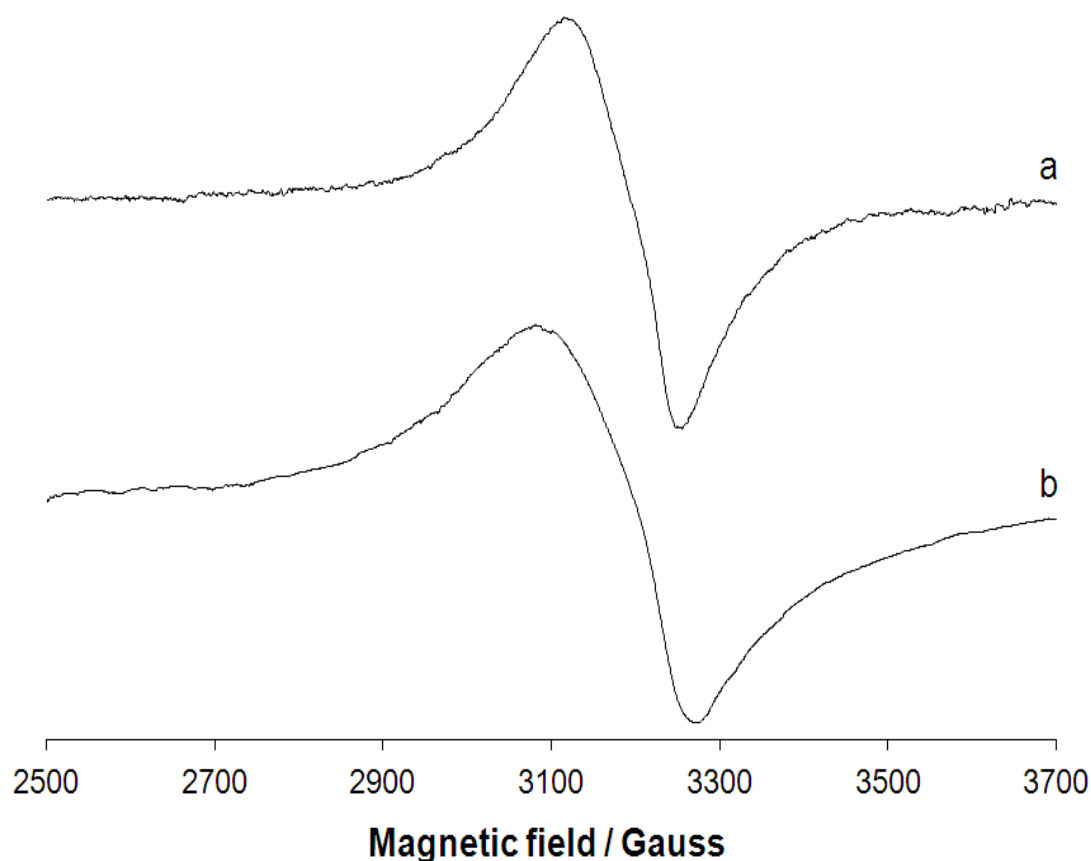


Figure 6. X-band EPR spectra of the polycrystalline complex **1** at: (a) 298 and (b) 77 K.

The EPR signal disappears almost completely when the solid complex **1** is dissolved in a coordinating solvent such as DMF (or DMSO, spectrum not shown) and in weakly coordinating solvent such as CH₃CN (**Figure 7**). This indicates a diamagnetic ground state with $S = 0$, which can be associated to a square planar geometry.⁴⁷ This means that in the presence of a coordinating solvent the two bridges are broken and mononuclear units are formed with the coordination of the tridentate ligand and a solvent molecule in the fourth equatorial position (**Scheme 1**). The tendency of polynuclear metal complexes to dissociate in solution is now a well-accepted fact in the literature and has been demonstrated in many cases, for example in the case of di- and polymeric Cu(II) species.⁴⁸

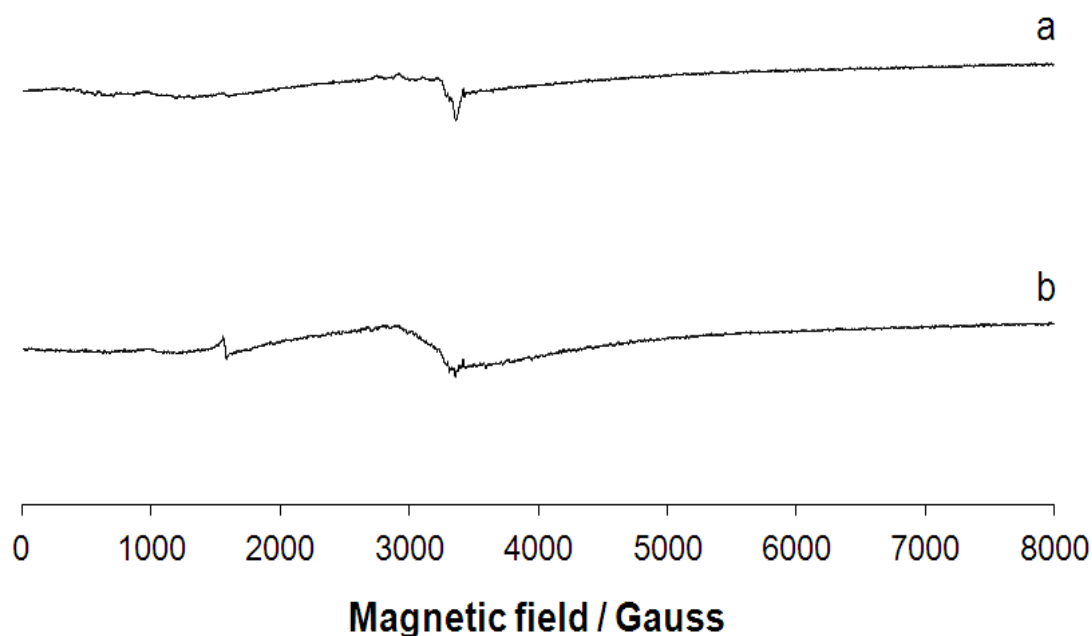
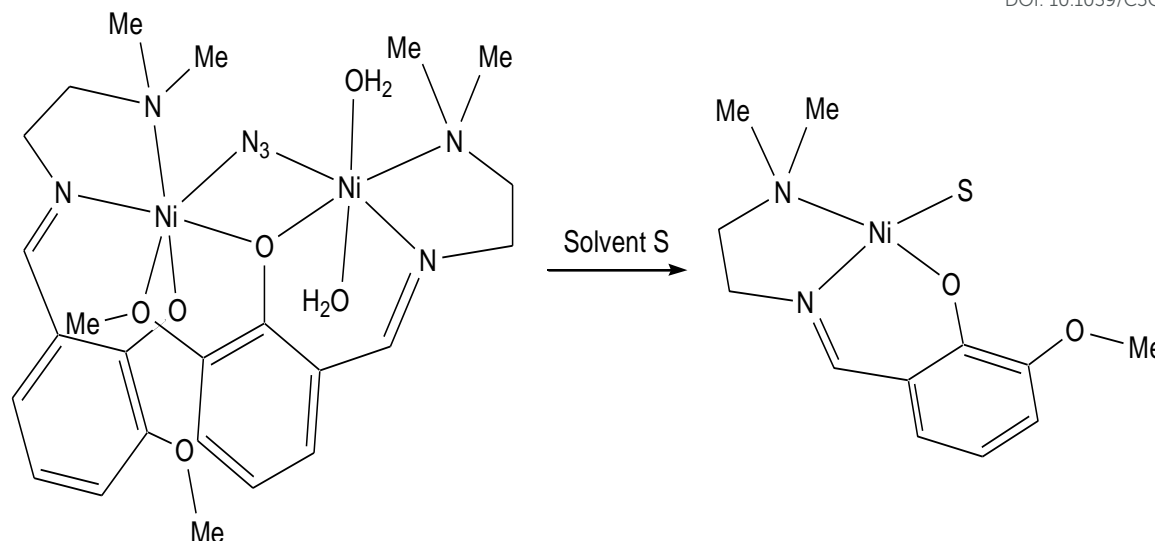


Figure 7. Anisotropic X-band EPR spectra of the complex **1** dissolved in: (a) DMF and (b) CH₃CN.



Scheme 1. Dissociation of complex **1** in the presence of a coordinating solvent S (S = DMF, DMSO, CH₃CN).

Magnetic moment

The temperature variation of the magnetic properties (in the temperature range from 5 to 300 K under an external field of 10,000 Oe) of complex **1** in the form of $\chi_m T$ vs. T (χ_m vs. T inset) plot is shown in **Figure 8** (χ_m is the molar susceptibility for two Ni(II)). At room temperature, the $\chi_m T$ value is 4.33 emu K G⁻¹ mol⁻¹. When lowering the temperature, the $\chi_m T$ value increases gradually to a maximum value of 5.82 emu K G⁻¹ mol⁻¹ at 18 K. It then decreases sharply with decreasing temperature and reaches a minimum of 4.81 emu K G⁻¹ mol⁻¹ at 5 K. This behaviour suggests that there is a ferromagnetic interactions between the bridging binuclear Ni(II) ions (S=1), because of the super-exchange interaction.

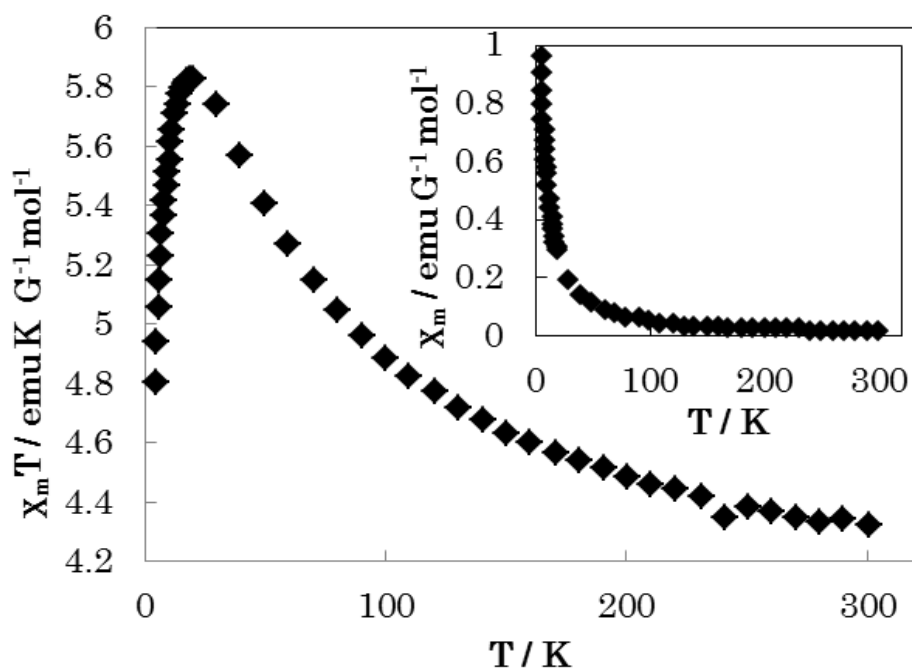


Figure 8. The temperature-dependent magnetic susceptibility data for **1** was measured in the temperature range from 5 to 300 K under an external field of 10,000 Oe.

Antimycobacterial activity

In the anti-mycobacterial assay, HL and complex **1** were tested against *M. tuberculosis* H37Rv and *M. tuberculosis* H37Ra strains as well as against two clinical strains (strain 1 and strain 2). The results are shown in **Table 5**. *M. tuberculosis* H37Rv and *M. tuberculosis* H37Ra, a well-known indicator, are used for the drug sensitivity tests.¹² The MIC and the MBC of HL to *M. tuberculosis* H₃₇Rv are 4 and 8 µg/mL, while the MIC and MBC of complex **1** are 8 µg/mL. Although HL shows the same MIC value against *M. tuberculosis* H₃₇Rv and *M. tuberculosis* H₃₇Ra, the MBC value against *M. tuberculosis* H₃₇Ra is higher than that against *M. tuberculosis* H₃₇Rv. On the other hand, the highest MIC and MBC values in the clinical isolates have been found for strain-1 (MIC 16 µg/mL and MBC 32 µg/mL) in the case of HL and for strain-2 (MIC 32 µg/mL and MBC 64 µg/mL) in the case of complex **1**. The results show that the compounds exhibit antimycobacterial activity against the tested drug resistant and drug susceptible *M. tuberculosis* strains with MIC at 4 µg/ml and MBC in the range of 8-16 µg/mL. Clinical strains are also affected by the compounds on the MIC 8-32 µg/mL and MBC 16-64 µg/mL (**Table 5**). Both HL and complex **1** show bactericidal activity. The ligand HL is more effective against drug resistant and drug susceptible *M. tuberculosis* and clinical isolates than complex **1** (**Figure 9**). In this study, we state that both compounds show a considerable efficacy on the Mycobacteria strains. The mycobacteria cell wall includes a large amount of complex lipids, lipopolysaccharides and mycolic acids. This constitution makes the cell wall a hydrophobic strong barrier against antimicrobial agents.⁴⁹

Table 5. Minimal inhibitory concentration (MIC) and minimal bactericidal concentration (MBC) of HL and complex 1 ($\mu\text{g/mL}$).

Compounds	Bacteria							
	Drug resistant and drug susceptible <i>M. tuberculosis</i>				Clinical isolates			
	H ₃₇ Rv		H ₃₇ Ra		Strain-1		Strain-2	
	MIC	MBC	MIC	MBC	MIC	MBC	MIC	MBC
HL	4	8	4	16	16	32	8	16
Complex 1	8	8	8	16	16	32	32	64
Concentrations of antimycobacterial drugs ($\mu\text{g/mL}$)								
Streptomisin	0.65	0.65	0.65	1.29	2.59	5.18	0.65	-
Isoniazid	0.13	1.03	0.51	1.03	0.51	1.03	0.51	0.51
Rifampicin	0.65	5.18	0.32	2.59	0.65	0.65	0.65	5.18
Ethambutol	3.744	7.48	1.87	1.87	3.74	3.74	1.87	-

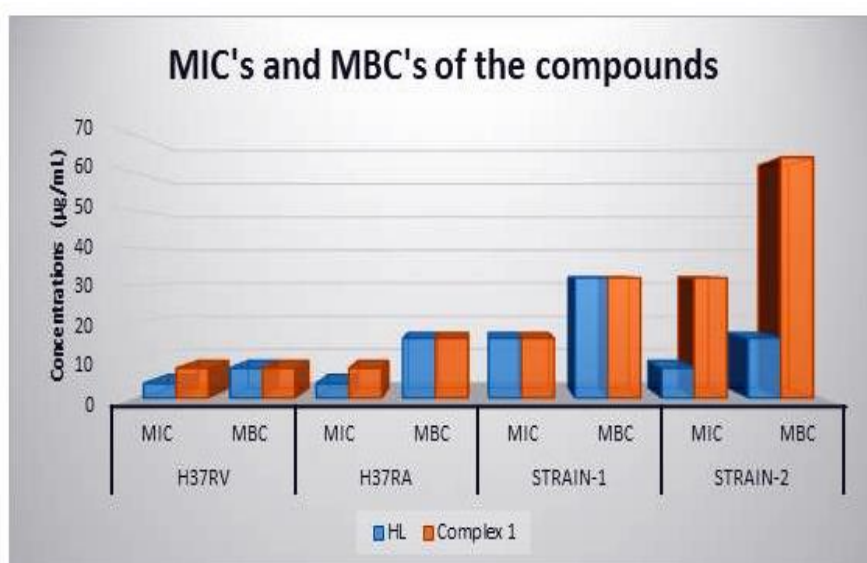


Figure 9. MIC's and MBC's of HL and complex 1.

Cytotoxicity study

The ligand, HL and complex **1** were investigated for cytotoxic effects on three cancer cell lines namely, A-549 (non-small cell lung cancer), MCF-7 (breast cancer), CaCo-2 (colon cancer cell line) and on one healthy cell line, CRL-2522 (human normal fibroblast). Generally, cytotoxic effects of the substances increase in conjunction with increase in concentration. While HL has $24.82 > 55.38 > 79.71$ $\mu\text{g/mL}$ downward IC₅₀ values on CaCo-2 > A-549 > MCF-7 respectively, it has the highest IC₅₀ value (306.75) on the healthy cell line CRL-2522 (see ESI, **Table S2**). This result is desirable for drug development methods and for that reason, HL is a candidate molecule for target drugs. CRL-2522 (human normal fibroblast) shows apoptotic effect under 1% on both IC₅₀ and IC₅₀/2 concentrations (**Figure 10**).

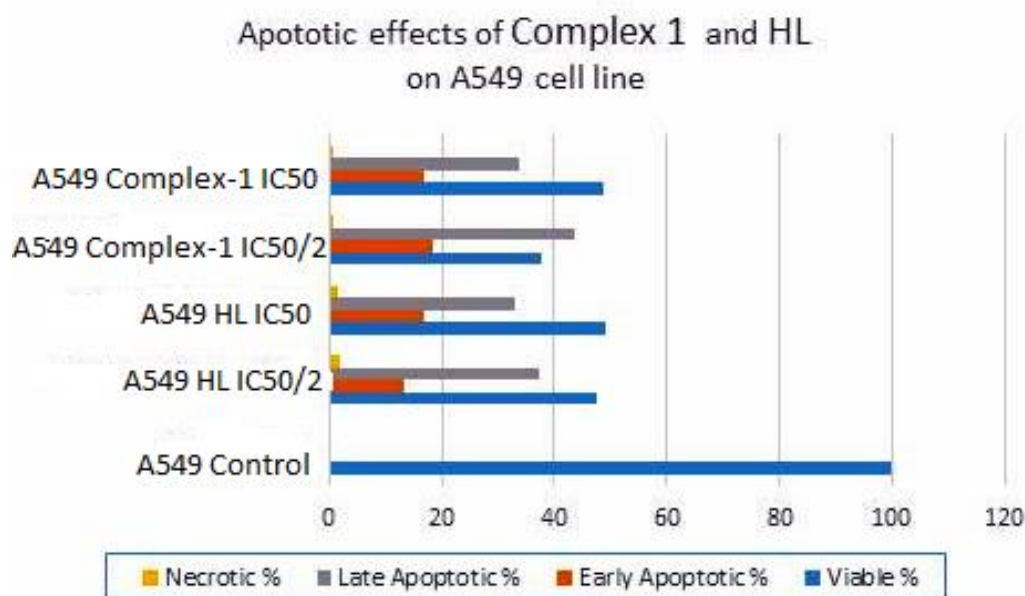


Figure 10. The ligand HL and complex **1** induced apoptosis in A-549 cells in a concentration-dependent fashion. In the case of MCF-7, Caco-2 and CRL-2522 cell lines, minimum apoptotic effects are obtained (data not shown).

Apoptosis detection by staining with Annexin V-fluorescein isothiocyanate and propidium iodide (FACS)

To determine and measure apoptotic events, the expression of phosphatidylserine at the cell surface is effected by flow cytometry (FCM) with Annexin-V-fluorescein isothiocyanate (FITC) and propidium iodide (PI). To study late apoptotic events, DNA strand breaks are determined compared with the PI.⁵⁰ The early apoptotic cells were Annexin V-positive and PI-negative, and the late apoptotic and dead cells were Annexin V-positive and PI-positive.⁵¹ In the IC₅₀ and exceed IC₅₀/2 concentrations of complex **1**, the total apoptosis rate exceeds 50% on A-549 cell lines. The MTT analysis indicates that complex **1** represses cell proliferation in a dose-subordinate procedure and this is confirmed by flow cytometric experiments using Annexin V-PI. The highest apoptotic rate is observed after treatment with IC₅₀/2 (21.05 µg/mL) on complex **1**. Circumstantially, the higher dosages (IC₅₀) of complex **1** (42.301 µg/mL) results in relatively lower apoptotic rates (see ESI, **Table S3**). CRL-2522 (human normal fibroblast) shows apoptotic effect under 1% on both IC₅₀ and IC₅₀/2 concentrations. Complex **1** could be considered as the best candidate for a drug active material since it needs a minimum concentration level to show cytotoxic activity on three cancer lines as well as being non-toxic even in high concentration on the healthy cell line fibroblast.

Docking study with enoyl acyl carrier protein reductase of *M.Tuberculosis* H37Rv

InhA, the enoyl acyl carrier protein reductase (ENR) from *M. tuberculosis* is one of the key enzymes involved in the mycobacterial fatty acid elongation cycle and has been validated as an effective antimicrobial target. Isoinazide is a well-known

tuberculosis drug that binds in the pocket of enoyl acyl carrier protein reductase and inhibits the action of fatty acid synthase. Pyrrolidine carboxamides⁵² are reported as a novel class of potent InhA inhibitors. By theoretical calculation we have tried to establish whether the ligand HL can act as a new InhA inhibitor. The crystallographic structures of the enoyl acyl carrier protein reductase of *M. tuberculosis* H37R_v and of the pyrrolidinium carboxamides complex were downloaded from RCSB protein data bank (PDB ID: 4U0K); they were resolved at 1.09 Å using X-Ray diffraction analysis. The energy-minimized structure of the ligand was used *in situ* for the protein-ligand docking studies in the cavity of the enzyme. To perform the docking study with HL and the enoyl acyl carrier protein reductase, we have selected the binding cavity of pyrrolidinium carboxamides. A total of fourteen amino acids (Ile21, Gly96, Phe97, Met98, Met103, Met147, Asp148, Phe149, Tyr158, Met161, Lys165, Ala193, Pro193, Met199) were present in the cavity sites. The ligand HL interacts with the protein forming two hydrogen bonds with Lys165 (1.94 and 2.53 Å, **Figures 11 and 12**). The relevant data of the docking study are given in **Tables 6 and 7**. The surface area of the active site cavity (with respect to the H-bond donor/acceptors) is depicted in **Figure 13**. We have removed the pyrrolidinium carboxamides from the binding cavity and docked inside the cavity. The best docked pose of the enoyl acyl carrier protein reductase and of pyrrolidinium carboxamides is comparable with the reported crystal data (4U0K) (see ESI, **Figure S4**). We have compared the Gibbs free energy of the protein-molecule complex for pyrrolidinium carboxamides and the ligand, HL. The protein-molecule complex for pyrrolidinium carboximide is slightly more stable than the the complex with the ligand (**Table 6**).

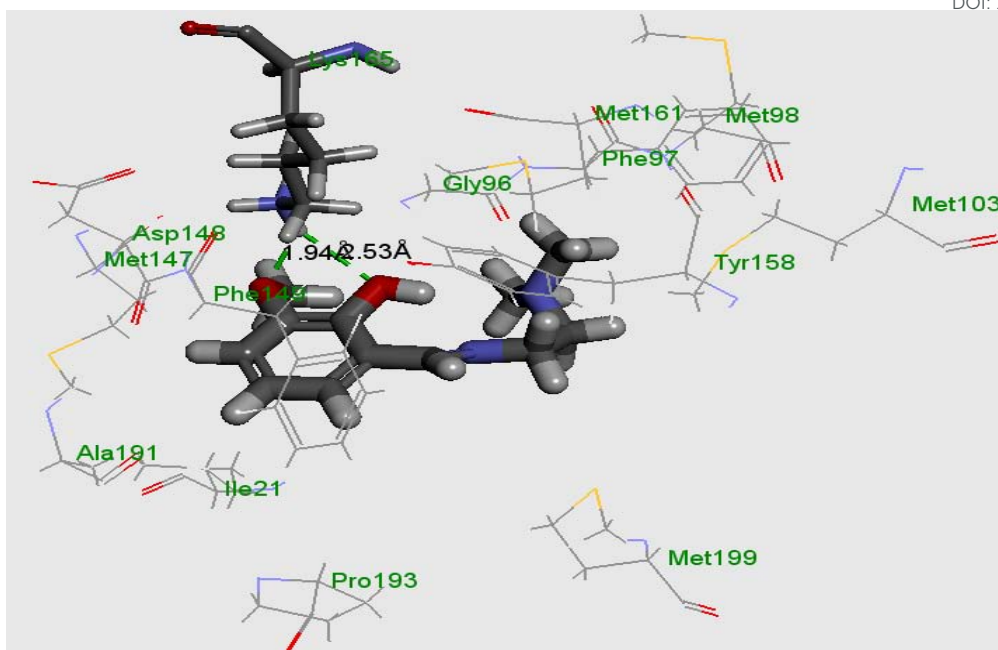


Figure 12. Best docked pose of the ligand (HL) inside the binding pocket of enoyl acyl carrier protein reductase (PDB id 4U0K) of *M. tuberculosis* H37R_v (2D view).

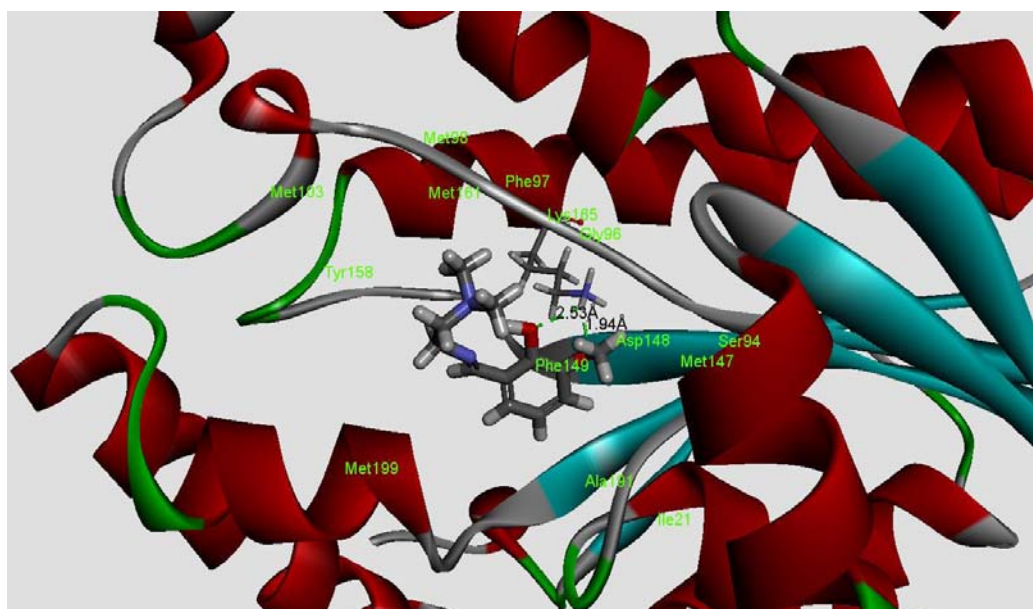


Figure 13. Best docked pose of the ligand (HL) (3D view) and the enoyl acyl carrier protein reductase (PDB id 4U0K) of *M. tuberculosis* H37R_v (3D view).

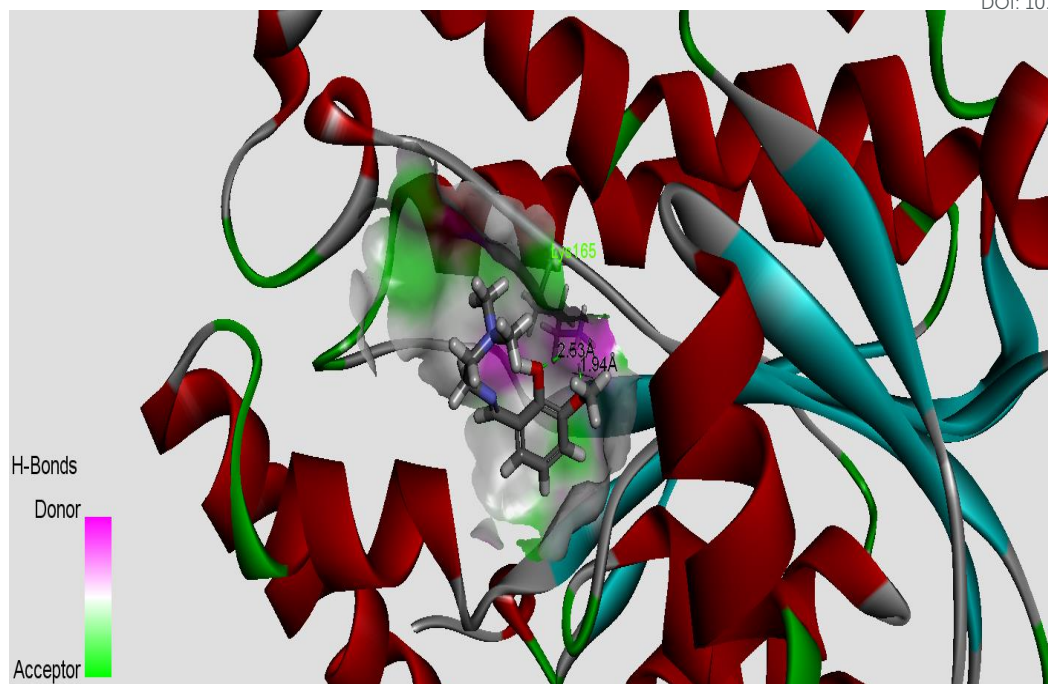


Figure 14. Surface area (with respect to the H-bond donors & acceptors) of the binding pocket in the best docked pose of ligand and protein.

Table 6. Details of the docking studies.

Compound	CDOCKER interaction energy	Energy of protein-molecule complex (Kcal/mol)	Ligand energy (Kcal/mol)	Protein energy (Kcal/mol)	Binding energy (Kcal/mol)
4U0K@ HL	-17.46	-10299.00	23.86	-10272.18	-50.67
4U0K@ pyrollidium carboxamides	-22.76	-10324.26	-12.58	-10272.18	-39.50

$$\text{Energy}_{\text{Binding}} = \text{Energy}_{\text{Complex}} - \text{Energy}_{\text{Ligand}} - \text{Energy}_{\text{Receptor}}$$

Table 7. Details of the interactions present in the most stable protein-ligand complex.

Compounds	Hydrogen bonds				
	No. of hydrogen bonds	End 1	End 2	Bond Distances Å	Angle DHA
HL	2	Lys165	O-atom of phenolic group	2.63	132.19
		Lys165	O-atom of methoxy group	1.94	126.43
Pyrollidium carboxamides	1	Tyr158	O-atom of carbonyl carbon	1.93	164.5

Druglikeness and ADMET prediction

Druglikeness and ADMET properties of HL have been checked following Lipinski's rule of five and the ADMET prediction module of Discovery studio 4.0. The ligand has passed the Lipinski's filter and according to the ADMET (absorption, distribution, metabolism, excretion and toxicity) prediction it is non-mutagenic and shows optimal druglikeness. Predicted data are summarized in **Table 8**.

Table 8. ADMET prediction for HL.

Compounds	Molecular Weight	ADMET Solubility (aqueous)	ADMET solubility level	ADMET absorption level [#]	ADMET _A logP98	No of H-bond acceptor	No. of H-bond donor	Lipinski's filter	Drug likeness inference	Ames Prediction
HL	222.84	-1.886	4	0 (good)	1.73	4	1	yes	yes, optimal	non-mutagen

[#] ADMET absorption level: 0, Good; 1, Moderate; 2, Low.

Conclusions

A potential tetradentate monoanionic N_2O_2 chelator, HL, is synthesized which affords the corresponding nickel derivative, $[Ni(L)(\mu_{1,1}-N_3)Ni(L)(OH_2)_2].ClO_4$ (**1**) (HL, [(2-[[2-(dimethylamino)ethyl]imino}methyl]-6-methoxyphenol]) when reacting with nickel perchlorate and sodium azide. The solid state structure of **1** shows that both the Ni atoms possess an octahedral N_3O_3 environment. The complex has been thoroughly characterized by means of different spectral analyses. The temperature dependent magnetic moment shows the existence of a ferromagnetic interactions between the bridging dinuclear Ni(II) ions. Both the ligand HL and complex **1** exhibit moderate anti-mycobacterial activity and considerable efficacy on the *M. tuberculosis* H37Rv ATCC 27294 and *M. tuberculosis* H37Ra ATCC 25177 strains. As regards to the cytotoxicity study, it has been proved that both the ligand and the complex respond well on cancer cell lines (A-549, MCF-7 and Caco-2), however; complex **1** shows low toxicity on healthy cell lines like CRL-2522. Further investigations in this area involving other metal ions integrated with new organic precursors, and considering the chemo-sensor activities of the ligands for selective detection of metal ions are currently being carried out in our laboratories.

Acknowledgements

KD and CS would like to thank West Bengal DST, Kolkata, India for the grant (228/1(10)/(Sanc.)/ST/P/S&T/9G-16/2012). AD would like to thank to The National Science Council, Taiwan for financial assistance. We also thank Mr. Kana Kobayashi for his valuable suggestions regarding the magnetic studies.

References

- 1 (a) P. Zanello, S. Tamburini, P. A. Vigato and G. A. Mazzochim, *Coord. Chem. Rev.*, 1987, **77**, 165-273; (b) P. A. Vigato, S. Tamburini and D. E. Fenton, *Coord. Chem. Rev.*, 1990, **106**, 25-170; (c) G. A. Morris, H. Zhou, C. L. Stern and S. T. Nguyen, *Inorg. Chem.*, 2001, **40**, 3222-3227; (d) N. N. Murthy, M. M. Tahir and K. D. Karlin, *J. Am. Chem. Soc.*, 1993, **115**, 10404-10405; (e) K. Bertocello, G. D. Fallon, J. H. Hodgkin and K. S. Murray, *Inorg. Chem.*, 1988, **27**, 4750-4758; (f) N. R. Sangeetha, C. K. Pal, P. Ghosh and S. Pal, *J. Chem. Soc., Dalton Trans.*, 1996, 3293-3296; (g) N. R. Sangeetha, K. Baradi, R. Gupta, C. K. Pal, V. Manivannan and S. Pal, *Polyhedron*, 1999, **18**, 1425-1429.
- 2 (a) S. H. Strauss, *Chem. Rev.*, 1993, **93**, 927-942; (b) S. O. Kang, R. A. Begum and K. Bowman-James, *Angew. Chem., Int. Ed.*, 2006, **45**, 7882-7884; (c) J. H. Han, J. W. Shin and K. S. Min, *Bull. Korean Chem. Soc.*, 2009, **30**, 1113-1117.
- 3 (a) S. K. Dey, N. Mondal, M. S. El Fallah, R. Vicente, A. Escuer, X. Solans, M. F. Bardia, T. Matsushita, V. Gramlich and S. Mitra, *Inorg. Chem.*, 2004, **43**, 2427-2434; (b) P. Talukder, A. Datta, S. Mitra, G. Rosair, M.S. El Fallah and J. Ribas, *Dalton Trans.*, 2004, 4161-4167; (c) N. K. Karan, S. Mitra, T. Matsushita, V. Gramlich and G. Rosair, *Inorg. Chim. Acta*, 2002, **332**, 87-91.
- 4 (a) S. Naiya, C. Biswas, M. G. B. Drew, C. J. G'omez-Garcia, J. M. Clemente-Juan and A. Ghosh, *Inorg. Chem.*, 2010, **49**, 6616-6627; (b) O. Sengupta and P. S. Mukherjee, *Inorg. Chem.*, 2010, **49**, 8583-8590; (c) O. Sengupta, G. Bappaditya, S. Mukherjee and P. S. Mukherjee, *Dalton Trans.*, 2010, **39**,

- 7451-7465; (d) K. C. Mondal, M. G. B. Drew and P. S. Mukherjee, *Inorg. Chem.*, 2007, **46**, 5625-5629.
- 5 E. Ruiz, J. Cano, S. Alvarez and P. Alemany, *J. Am. Chem. Soc.*, 1998, **120**, 11122-11129.
- 6 (a) C. P. Landee and R. D. Willett, *Inorg. Chem.*, 1981, **20**, 2521-2525; (b) J. C. Jansen, H. van Koningsveld, J. A. C. van Ooijen and J. Reedijk, *Inorg. Chem.*, 1980, **19**, 170-174; (c) R. J. Butcher and E. Sinn, *Inorg. Chem.*, 1977, **16**, 2334-2343; (d) H. S. Preston and C. H. L. Kennard, *J. Chem. Soc. A*, 1969, 2682-2686.
- 7 (a) A. P. Ginsberg, R. L. Martin, R. W. Brookes and R. C. Sherwood, *Inorg. Chem.*, 1972, **11**, 2884-2889; (b) T. Rojo, L. Lezama, R. Cortes, J. L. Mesa, M. I. Arriortua and G. Villeneuve, *J. Magn. Mater.*, 1990, **83**, 519-521.
- 8 O. Kahn, *Inorg. Chim. Acta*, 1982, **62**, 3-14.
- 9 (a) N. Mondal, S. Mitra, V. Gramlich, S. O. Ghodsi and K. M. A. Malik, *Polyhedron*, 2001, **20**, 135-141; (b) M. Amirnasr, K. J. Schenk, S. Meghdadi and M. Morshedi, *Polyhedron*, 2006, **25**, 671-677.
- 10 A. L. Okunade and M. P. F. Elvin-Lewis, *Phytochem.*, 2004, **65**, 1017-1032.
- 11 N. Lall, M. D. Sarma, B. Hazra and J. J. Meyer, *J. Antimicro. Chem.*, 2003, **51**, 435-438.
- 12 E. Banfi, M. G. Mamolo, D. Zampieri, L. Vio and C. M. Bragadin, *J. Antimicro. Chem.*, 2001, **48**, 705-711.
- 13 E. Vattemi and P. P. Claudio, *Drug News Perspect.*, 2007, **20**, 511-520.
- 14 K. C. Zimmermann, C. Bonzon and D. R. Green, *Pharmacol. Ther.*, 2001, **92**, 57-70.

- 15 (a) N. A. Thornberry, T. A. Rano, E. P. Peterson, D. M. Rasper, T. Timkey, M. Garcia-Calvo, V. M. Houtzager, P. A. Nordstrom, S. Roy, J. P. Vaillancourt, K. T. Chapman and D. W. Nicholson, *J. Biol. Chem.*, 1997, **272**, 17907-17911; (b) A. Marin-Hernandez, I. Gracia-Mora, L. Ruiz-Ramirez and R. Moreno-Sanchez, *Biochem. Pharmacol.*, 2003, **65**, 1979-1989.
- 16 R. Koner, S. Hazra, M. Fleck, A. Jana, C. R. Lucas and S. Mohanta, *Eur. J. Inorg. Chem.*, 2009, 4982-4988.
- 17 (a) S. Sen, P. Talukder, S. K. Dey, S. Mitra, G. Rosair, D. L. Hughes, G. P. A. Yap, G. Pilet, V. Gramlich and T. Matsushita, *Dalton Trans.*, 2006, 1758-1767; (b) S. Basak, S. Sen, S. Banerjee, S. Mitra, G. Rosair and M. T. G. Rodriguez, *Polyhedron*, 2007, **26**, 5104-5112; (c) C. R. Choudhury, S. K. Dey, R. Karmakar, C.-D. Wu, C.-Z. Lu, M. S. El Fallah and S. Mitra, *New J. Chem.*, 2003, **27**, 1360-1366; (d) G. Das, R. Shukla, S. Mandal, R. Singh, P. K. Bharadwaz, *Inorg. Chem.*, 1997, **36**, 323-329.
- 18 D. F. Eaton, *Pure & Appl. Chem.*, 1988, **60**, 1107-1114.
- 19 S. R. Stoyanov, J. M. Villegas and D. P. Rillema, *Inorg. Chem.*, 2002, **41**, 2941-2945.
- 20 (a) SADABS Bruker AXS; Madison, Wisconsin, USA, 2004; SAINT, *Software Users Guide, Version 6.0*; Bruker Analytical X-ray Systems, Madison, WI, 1999; (b) G. M. Sheldrick, SADABS v2.03: *Area-Detector Absorption Correction*. University of Göttingen, Germany, 1999.
- 21 A. Altomare, M. C. Burla, M. Camalli, G. L. Cascarano, C. Giacovazzo, A. Guagliardi, A. G. G. Moliterni, G. Polidori and R. Spagna, *J. Appl. Crystallogr.*, 1999, **32**, 115-119.
- 22 G. M. Sheldrick, *Acta Cryst.*, 2008, **A64**, 112-122.

- 23 L. J. Farrugia, *J. Appl. Crystallogr.*, 1999, **32**, 837-838.
- 24 C. Lee, W. Yang and R.G. Parr, *Phys. Rev.*, 1988, **B37**, 785-789.
- 25 M. J. Frisch, G. W. Trucks, H. B. Schlegel, G. E. Scuseria, M. A. Robb, J. R. Cheeseman, J. A. Montgomery Jr., T. Vreven, K. N. Kudin, J. C. Burant, J. M. Millam, S. S. Iyengar, J. Tomasi, V. Barone, B. Mennucci, M. Cossi, G. Scalmani, N. Rega, G. A. Petersson, H. Nakatsuji, M. Hada, M. Ehara, K. Toyota, R. Fukuda, J. Hasegawa, M. Ishida, T. Nakajima, Y. Honda, O. Kitao, H. Nakai, M. Klene, X. Li, J. E. Knox, H. P. Hratchian, J. B. Cross, V. Bakken, C. Adamo, J. Jaramillo, R. Gomperts, R. E. Stratmann, O. Yazyev, A. J. Austin, R. Cammi, C. Pomelli, J. W. Ochterski, P. Y. Ayala, K. Morokuma, G. A. Voth, P. Salvador, J. J. Dannenberg, V. G. Zakrzewski, S. Dapprich, A. D. Daniels, M. C. Strain, O. Farkas, D. K. Malick, A. D. Rabuck, K. Raghavachari, J. B. Foresman, J. V. Ortiz, Q. Cui, A. G. Baboul, S. Clifford, J. Cioslowski, B. B. Stefanov, G. Liu, A. Liashenko, P. Piskorz, I. Komaromi, R. L. Martin, D. J. Fox, T. Keith, M. A. Al-Laham, C. Y. Peng, A. Nanayakkara, M. Challacombe, P. M. W. Gill, B. Johnson, W. Chen, M. W. Wong, C. Gonzalez and J. A. Pople, GAUSSIAN 03 Revision D 01, Gaussian Inc., Wallingford, CT, 2004.
- 26 GaussView3.0, Gaussian: Pittsburgh, PA.
- 27 P. J. Hay and W. R. Wadt, *J. Chem. Phys.*, 1985, **82**, 270-283.
- 28 R. Bauernschmitt and R. Ahlrichs, *Chem. Phys. Lett.*, 1996, **256**, 454-464.
- 29 M. K. Casida, C. Jamorski, K. C. Casida and D. R. Salahub, *J. Chem. Phys.*, 1998, **108**, 4439-4449.
- 30 R. E. Stratmann, G. E. Scuseria and M. J. Frisch, *J. Chem. Phys.*, 1998, **109**, 8218-8224.

- 31 M. Cossi, N. Rega, G. Scalmani and V. Barone, *Comput. Chem.*, 2003, **24**, 669-681.
- 32 N. M. O'Boyle, A. L. Tenderholt and K. M. Langner, *J. Comput. Chem.*, 2008, **29**, 839-845.
- 33 B. D. Becton, Dickinson and Company Newsletter BD Bactec MGIT 960 SIRE kit now FDA-cleared for susceptibility testing of Mycobacterium tuberculosis. *Microbiology News & Ideas* 13: 4-4, 2002.
- 34 NCCLS, (2003). National Committee for Clinical Laboratory Standards (NCCLS). Susceptibility Testing of Mycobacteria, Nocardiae, and Other Aerobic Actinomycetes; Approved Standard. NCCLS document M24-A [ISBN 1-56238-500-3]. NCCLS, 940 West Valley Road, Suite 1400, Wayne, Pennsylvania 19087-1898 USA, 2003.
- 35 L. Collins and S. G. Franzblau, *Antimicro. Agents Chemother.*, 1997, **41**, 1004-1009.
- 36 A. Jimenez-Arellanes, M. Meckes, R. Ramirez, J. Torres and J. Luna-Herrera, *Phytother. Res.*, 2003, **17**, 903-908.
- 37 (a) G. R. Battu and B. M. Kumar, *Willd. Pharmacognosy J.*, 2010, **2**, 456-463;
(b) P. Bontempo, V. Carafa, R. Grassi, A. Basile, G. C. Tenore, C. Formisano, D. Rigano and L. Altucci, *Food Chem. Toxicology*, 2013, 304-312.
- 38 T. Mosman, *J. Immunol. Methods*, 1983, **65**, 55-63.
- 39 C. A. Lipinski, F. Lombardo, B. W. Dominy and P. J. Feeney, *Adv. Drug Delivery Rev.*, 2001, **46**, 3-26.
- 40 C. A. Lipinski, *Drug discovery today: Technologies*, 2004, **1**, 337-341.
- 41 Discovery Studio 4.0 is a product of Accelrys Inc, San Diego, CA, USA.

- 42 K. Nakamoto, *Infrared and Raman Spectra of Inorganic and Coordination Compounds, Parts A and B*, 5th Ed., John Wiley, New York, 1997.
- 43 S. Ferrer, J. G. Haasnoot, J. Reedijk, E. Muller, M. B. Cingi, M. Lanfranchi, A. M. M. Lanfredi and J. Ribas, *Inorg. Chem.*, 2000, **39**, 1859-1867.
- 44 A. B. P. Lever, *Inorganic Electronic Spectroscopy*, second ed., Elsevier, New York, 1984.
- 45 (a) J. L. Kropp, M. W. Windsor, *J. Chem. Phys.*, 1963, **39**, 2769-2770; (b) J. L. Kropp, M. W. Windsor, *J. Chem. Phys.*, 1965, **42**, 1599-1608.
- 46 A. Bencini and D. Gatteschi, In *Transition Metal Chemistry*, Melson, G. A.; Figgis, B. N., Eds. Marcel Dekker: New York, 1982; Vol. 8, pp 1-178.
- 47 F. A. Cotton, G. Wilkinson, C. A. Murillo and M. Bochmann, *Advanced Inorganic Chemistry, Sixth Edition*. John Wiley & Sons, Inc.: New York, 1999.
- 48 (a) J. C. Jeffery, J. P. Maher, C. A. Otter, P. Thornton and M. D. Ward, *J. Chem. Soc., Dalton Trans.*, 1995, 819-824; (b) W. A. Alves, R. H. A. Santos, A. Paduan-Filho, C. C. Becerra, A. C. Borin A. M. D. C. Ferreira, *Inorg. Chim. Acta*, 2004, **357**, 2269-2278; (c) M. A. Ali, A. H. Mirza, R. J. Fereday, R. J. Butcher, J. M. Fuller, S. C. Drew, L. R. Gahan, G. R. Hanson, B. Moubaraki and K. S. Murray, *Inorg. Chim. Acta*, 2005, **358**, 3937-3948; (d) I. A. Koval, M. Sgobba, M. Huisman, M. Lüken, E. Saint-Aman, P. Gamez, B. Krebs and J. Reedijk, *Inorg. Chim. Acta*, 2006, **359**, 4071-4078; (e) S. Thakurta, J. Chakraborty, G. Rosair, J. Tercero, M. S. El Fallah, E. Garribba and S. Mitra, *Inorg. Chem.*, 2008, **47**, 6227-6235; (f) S. Thakurta, P. Roy, G. Rosair, C. J. Gomez-Garcia, E. Garribba and S. Mitra, *Polyhedron*, 2009, **28**,

- 695-702; (g) S. Saha, A. Sasmal, C. R. Choudhury, C. J. Gomez-Garcia, E. Garribba and S. Mitra, *Polyhedron*, 2014, **69**, 262-269.
- 49 (a) D. E. Minnikin, M. Goodfellow, in *microbiological classification and identification*; R.G. Board, Eds.; Academic: London, 1980; p 189. (b) D. E. Minnikin, *Lipids; complex lipids, their chemistry, biosynthesis and roles*. In *The biology of mycobacteria*. C. Ratledge and J. Stanford, Eds.; London; Academic Press, Inc., 1982, p 95.
- 50 M. Martinez-Losa, J. Cortijo, G. Juan, M. Ramón, M. J. Sanz and E. J. Morcillo, *Modulatory effects of N-acetyl-L-cysteine on human eosinophil apoptosis*, *ERJ*, 2007, 30, p436.
- 51 T. Nakanoma, M. Ueno, M. Iida, R. Hirata and N. Deguchi, *Int. J. Urol.*, 2001, **8**, 623-630.
- 52 X. He, A. Alian, R. Stroud and P. R. Ortiz de Montellano, *J. Med. Chem.*, 2006, **49**, 6308-6323.

